NEOPLASIA
www.neoplasia.com
Volume 22 Number 2 October 2020 pp. 120-128

Original Research

Alterations in signaling pathways that accompany spontaneous transition to malignancy in a mouse model of BRAF mutant microsatellite stable colorectal cancer

Alexandra M. Kane [a,b,c,*]; Lochlan J. Fennell [a,b]; Cheng Liu [a,b,d]; Jennifer Borowsky [a,b]; Diane M. McKeone [a]; Catherine E. Bond [a]; Stephen Kazakoff [a]; Ann-Marie Patch [a]; Lambros T. Koufariotis [a]; John Pearson [a]; Nicola Waddell [a]; Barbara A. Leggett [a,b,e]; Vicki L.J. Whitehall [a,b,c]

[a] QIMR Berghofer Medical Research Institute, Brisbane, Queensland, Australia; [b] The University of Queensland, Brisbane, Queensland, Australia; [c] Conjoint Internal Medicine Laboratory, Pathology Queensland, Queensland Health, Brisbane, Queensland, Australia ; [d] Envoi Specialist Pathologists, Brisbane, Queensland, Australia; [e] The Royal Brisbane and Women's Hospital, Queensland Health, Brisbane, Queensland, Australia

Abstract

The serrated neoplasia pathway gives rise to a distinct subgroup of colorectal cancers distinguished by the presence of mutant *BRAF*^{V600E} and the CpG Island Methylator Phenotype (CIMP). *BRAF* mutant CRC are commonly associated with microsatellite instability, which have an excellent clinical outcome. However, a proportion of *BRAF* mutant CRC retain microsatellite stability and have a dismal prognosis. The molecular drivers responsible for the development of this cancer subgroup are unknown. To address this, we established a murine model of *BRAF*^{V600E} mutant microsatellite stable CRC and comprehensively investigated the exome and transcriptome to identify molecular alterations in signaling pathways that drive malignancy. Exome sequencing of murine serrated lesions (mSL) and carcinomas identified frequent hot spot mutations within the gene encoding β-catenin (*Ctnnb1*). Immunohistochemical staining of β-catenin indicated that these mutations led to an increase in the presence of aberrant nuclear β-catenin that resulted in gene expression changes in targets of β-catenin transcription. Gene expression profiling identified a significant enrichment for transforming growth factor-β (TGF-β) signaling that was present in mSL and carcinomas. Early activation of TGF-β suggests that this pathway may be an early cue directing mSL to microsatellite stable carcinoma. These findings in the mouse model support the importance of alterations in WNT and TGF-β signaling during the transition of human sessile serrated lesions to malignancy.

Neoplasia (2020) xx xxx–xxx

Keywords: *BRAF*, Colorectal cancer, WNT, TGF-β, Microsatellite

Introduction

The development of colorectal cancer (CRC) occurs through a multistep process from adenoma to carcinoma that is accompanied by genetic and epigenetic alterations [1]. The serrated neoplasia pathway describes an alternative pathway to the development of CRC [2,3]. Early premalignant lesions, sessile serrated lesions (SSL, formerly sessile serrated adenoma), represent a molecularly and histologically distinct subtype of polyp within the colon. The majority of SSL harbor a *BRAF*^{V600E} mutation and accumulate DNA hypermethylation resulting in the acquisition

Abbreviations: CIMP, CpG island methylator phenotype, CRC, colorectal cancer, HP, hyperplasia, MSI, microsatellite instability, MSS, microsatellite stable, mSL, murine serrated lesion, SSL, sessile serrated lesion, TGF-β, transforming growth factor-β, WT, wild type

* Corresponding author at: QIMR Berghofer Medical Research Institute, 300 Herston Road Herston, Queensland 4006, Australia
e-mail address: Alexandra.Kane@qimrberghofer.edu.au (A.M. Kane).

https://doi.org/10.1016/j.neo.2019.12.002

of the CpG islander methylator phenotype (CIMP) [4,5]. While methylation-induced silencing of *MLH1* and consequential development of microsatellite instability (MSI) commonly occurs, approximately 25% of dysplastic SSL retain MLH1 protein expression and are microsatellite stable (MSS) [5–7]. These lesions progress to malignancy via unknown mechanisms. Determining microsatellite stability status has implications for patient outcomes, with MSI cancers having improved response to immunotherapies and an excellent prognosis [6]. In contrast, *BRAF* mutant MSS CRC is associated with late-stage presentation, an aggressive phenotype and poor patient prognosis [6,8]. Understanding the genetic alterations that drive SSL to this aggressive subtype of cancer would identify further treatment strategies for affected patients.

To address this we have established a genetically modified mutant $Braf^{V637E}$ murine model, analogous to human $BRAF^{V600E}$ mutation, that mimics the serrated neoplasia pathway observed in humans [9]. Following cre-mediated activation of mutant $Braf^{V637E}$ in the intestine, all mice immediately develop persistent hyperplasia throughout the intestine, characterized by diffuse villous elongation and cellular crowding. Murine serrated lesions (mSL) develop in the proximal small intestine after 8 months and resemble human SSL with dilatated glands at the crypt bases. By 14 months, invasive carcinomas arise within the background mSL in approximately 30% of mice. These carcinomas produce liver or peritoneal metastases in approximately 40% of cancer cases. We have shown that these carcinomas do not methylate *MLH1*, retain MLH1 protein expression and are MSS, which is in contrast to that previously published by Rad and colleagues [10].

In this study, we aimed to characterize the molecular alterations that occur following mutation of $Braf^{V637E}$ during the natural progression of serrated neoplasia. We collected samples from mice representing the evolution of histological phenotypes, including wild type mucosa, hyperplasia, mSL and carcinomas. Exome and RNA sequencing were performed to investigate genomic and transcriptional changes that drive malignancy. Integrating both genetic and transcriptional analyses will contribute to understanding the molecular characteristics of human *BRAF* mutant MSS CRC and highlight potential therapeutic targets.

Materials and methods

Braf mutant mice and sample collection

$Braf^{V637E/+}$/*Villin-Cre*$^{ERT2/+}$ mice were generated to express mutant $Braf^{V637E}$, equivalent to human $BRAF^{V600E}$ mutation, within the intestine as previously described [9]. At 14 days, intestinal specific mutant $Braf^{V637E}$ activation was achieved via a single intraperitoneal injection of tamoxifen (75 mg/kg, Sigma-Aldrich, MO, USA). *Braf* mutant and wild type littermates were aged to 10 and 14 months, at which point animals were euthanized. The gastrointestinal tract was excised and evaluated for the presence of mSL and carcinoma. Samples of hyperplasia, mSL or carcinoma were collected from the proximal small intestine of *Braf* mutant mice. Histological diagnosis of mSL and carcinoma were performed by a gastrointestinal pathologist (CL). Samples of hyperplasia were collected a minimum of five centimeters away from the site of any lesion. Normal mucosa was sampled from the proximal small intestine of wild type littermates. All sampling was performed by scraping the cells of the mucosa, enriching for epithelial cells, before immediately being snap frozen in liquid nitrogen.

Genomic DNA and RNA was extracted from tissue using Qiagen AllPrep kits (Qiagen, CA, USA) and subjected to exome and RNA sequencing. DNA and RNA quality was assessed using QuBit BR dsDNA assay kit (Thermofisher, MA, USA) and Agilent TapeStation system (Agilent Technologies, CA, USA), respectively. Numbers of samples collected at each time point for differing morphology are summarized in Supplementary Table 1.

Exome sequencing

Exome sequencing was performed on gDNA extracted from 12 mSL and 6 carcinomas, including 5 mSL from mice 10 months post induction of the *Braf* mutation and 7 mSL and 6 carcinomas from mice 14 months post *Braf* mutation. Matched hyperplastic mucosa was chosen as germline control to identify somatic mutations contributing to serrated pathology, filtering mutations in hyperplastic cells that have not contributed to progression of malignancy. Exome capture was achieved using Agilent SureSelect XT Mouse All Exon library kit (Agilent Technologies, CA, USA). Sequencing was performed on the HiSeq4000 platform (Illumina, CA, USA) producing 100 bp paired-end reads at 100X coverage for hyperplastic mucosa and 200X coverage for mSL and carcinoma.

Sequence reads were trimmed using Cutadapt (v1.9) [11], aligned to GRCm38/mm10 with BWA-MEM (v0.7.12) [12], duplicate-marked with Picard (v1.129, https://broadinstitute.github.io/picard/) and coordinate-sorted using Samtools (v1.1) [13]. Single nucleotide substitution variants were detected using a dual calling strategy using qSNP (v2.0) [14] and the GATK HaplotypeCaller (v3.3-0) [15]. The HaplotypeCaller was also used to call short indels of $\leq$50 base pairs. Initial read quality filtering for all variants detected included: a minimum of 35 bases in the CIGAR string indicated a match, 3 or fewer mismatches in the sequencing MD field, and a mapping quality greater than 10. High confidence variants were selected based on passing further variant characteristic filtering requirements and were used in all downstream analyses. These filtering requirements were: a minimum coverage of 8 reads in the control data and 12 reads in the tumour data; at least 5 variant supporting reads present where the variant was not within the first or last 5 bases; at least 4 of the 5 reads with unique start positions; the variant was identified in reads of both sequencing directions; the variant was not less than 5 base pairs from a mono-nucleotide run of 7 or more bases in length. Variants were annotated with gene feature information and transcript or protein consequences using SnpEff (v4.0e) [16]. Results for synonymous variants were filtered and removed.

RNA sequencing

RNA was extracted from 5 wild type mucosa samples, 12 hyperplastic mucosa samples, 18 mSL and 6 carcinomas for RNA sequencing. These 41 samples were collected from 41 mice to maintain statistical independence.

RNA for sequencing was prepared using Truseq standard mRNA library preparation kit (Illumina, CA, USA) and sequenced on the Nextseq 550 platform (Illumina, CA, USA) producing 75 base pair paired-end reads. Samples were sequenced to a mean depth of 54,770,529 reads per sample. The sequence reads were adapter trimmed using Cutadapt (v1.9) [11] and aligned with STAR (v2.5.2a) [17] to the GRCm38 assembly with the gene, transcript, and exon features of the Ensembl gene model (release 70). Quality control metrics were computed using RNA-SeQC (v1.1.8) [18] and gene and isoform counts were estimated using RSEM (v1.2.30) [19].

Single sample gene set enrichment analysis was performed as previously described with Wilcoxon Rank Sum Test and False Discovery Rate correction used to determine statistical significance [20]. Differential gene expression analysis was performed between each histological phenotype using the DEseq2 (v3.8) package [21]. Differentially expressed genes with a FDR corrected P-value < 0.05 and absolute $\log_2$ fold change (FC) $\geq$ 2 were considered significant. Data in figures is presented in fragments per kilobase of transcript per million mapped reads (FPKM).

Immunohistochemistry

Immunohistochemical staining for β-catenin was performed on dewaxed and rehydrated 4 μm sections cut from formalin-fixed, paraffin-embedded blocks. Antigen retrieval was performed by heat-induced epitope retrieval in a decloaking chamber using Dako high antigen retrieval solution (pH 9.0, Agilent Technologies, CA, USA) at 121 °C for 8 minutes. Following peroxidase blocking with 5% H_2O_2 and incubation with Background Sniper (Biocare Medical, CA, USA), sections were then stained for β-catenin using primary rabbit monoclonal anti-β-catenin antibody (1:500, Abcam, Cambridge, UK) overnight at room temperature. MACH1 Universal Polymer HRP detection system (Biocare Medical, CA, USA) was applied for one hour before incubation with 3,3′-diaminobenzidine and counter-staining with Mayer's hematoxylin.

Grading of β-catenin localization was performed by a gastrointestinal pathologist (JB) who assessed cases for aberrant staining, indicated by a shift from membranous to nuclear labeling. Nuclear staining was assessed for both intensity and extent of staining throughout the lesion as previously described [22,23]. Nuclear intensity was given an average score 0–3 (0 = no staining, 1 = weak staining, 2 = moderate staining, 3 = strong staining). Nuclear extent was scored as 0–4 (0 = no nuclei, 1 = 1–10% of nuclei, 2 = 11–50% nuclei, 3 = 51–90% nuclei, 4 = >90%). A final overall nuclear score was calculated by multiplying the individual scores for intensity and extent. Lesions with an abnormal staining pattern for β-catenin required an overall nuclear score of $\geq$2. The overall nuclear score was then assigned a qualitative score based on the following categories: 0 = no expression; 1–4 = low expression; 5–8 = moderate expression; and 9–12 = high expression. Fisher's exact test was used to determine significance of categorical variables.

Results

Exome sequencing shows recurrent somatic mutations in Ctnnb1

Exome sequencing was performed on a subset of mSL and carcinomas to identify somatic mutations. A total of 831 genes had non-synonymous mutations in at least one lesion, that included 735 missense mutations, 23 insertions or deletions and 16 non-sense mutations. The number of variants per sample ranged from 4 to 164 with a median of 24 variants per samples (Figure 1A). There were few recurrent mutations present with only 44 genes mutated in two or more samples (Figure 1B, Supplementary Table 2). *Ctnnb1,* encoding the intracellular WNT signaling protein β-catenin, was the most frequently mutated gene with a mutation present in 16 of 18 samples (89%, Table 1). *Ctnnb1* was mutated in 4/5 (80%) mSL sampled from mice aged to 10 months post activation of *Braf* mutation with one mSL having two missense mutations present. At 14 months, *Ctnnb1* mutations were present in 7/7 (100%) mSL and 5/6 (83%) carcinomas. Mutations were frequently missense (15/17, 88%) occurring within exon 3 at known hot-spot locations at codons 32, 33, 37 and 41. Additionally, there were 2 samples with in-frame deletions in exon 3.

Mutations at those respective codons within exon 3 of *Ctnnb1* result in the accumulation of β-catenin within the nucleus where it acts as a proto-oncogene driving transcription of target genes [24]. To determine that mutation of *Ctnnb1* resulted in altered cellular localization of β-catenin we performed immunohistochemistry. β-catenin stained sections of mSL and carcinoma were assessed for nuclear translocation (Figure 2C–F), which differs from the cell membrane staining pattern that occurs in the absence of WNT signaling activation (Figure 2A and B). Abnormal nuclear β-catenin was found in 2/5 (40%) of mSL at 10 months (Table 1). A common staining pattern was strong nuclear staining in 1–10% of the cells in the lesion. This may account for the discrepancies in 2 samples having mutation but no nuclear staining due to the small number of cells within the lesion having abnormal nuclear staining pattern. At 14 months, 7/7 (100%) mSL and 6/6 (100%) of carcinomas had positive nuclear β-catenin (Table 1). When comparing mSL versus carcinoma, carcinomas had a significantly higher score (P = 0.0039) with these lesions having on average >50% of cells with nuclear β-catenin. One carcinoma on exome sequencing was wild type for β-catenin mutation, however on immunohistochemical staining had abnormal nuclear translocation. In this case, activation of WNT signaling and translocation of β-catenin may be due to other mechanisms, such as methylation-induced silencing of negative WNT regulators.

Gene expression changes in serrated neoplasia

As there were minimal other recurrent mutations present in mSL and carcinomas, we performed RNA sequencing to examine gene expression changes that occurred during the progression of serrated neoplasia. We applied principal components analysis to determine if changes in gene expression could delineate histological phenotypes. This analysis showed clear distinction between wild type mucosa and hyperplasia from mSL

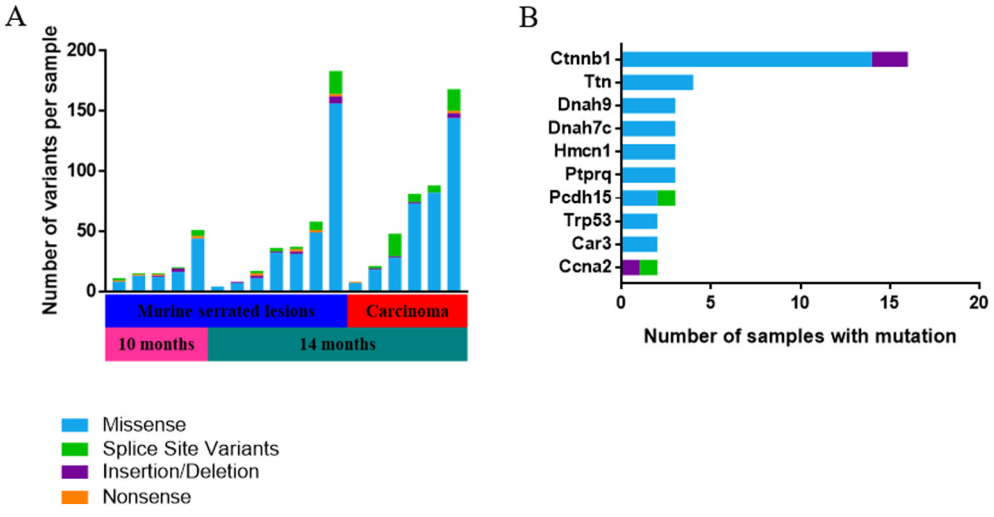

Figure 1. Summary of exome sequencing data showing the number of non-synonymous variants per sample (A) and top 10 most frequently mutated genes per sample (B).

Table 1. *Ctnnb1* mutations and β-catenin immunohistochemical staining of mSL and carcinomas sampled from mice at 10 and 14 month post activation of mutant $Braf^{V637E.}$

Time post activation of $Braf^{V637E}$	Histology	Nucleotide Change	Codon Change	β-catenin Staining	Score
10 months	Murine serrated lesion	c.122C > T	p.Thr41Ile	Nuclear	3
		c.98C > T c.122C > T	p.Ser33Phe p. Thr41Ile	Nuclear	3
		c.98C > T	p.Ser33Phe	Membranous	0
		c.110C > T	p.Ser37Phe	Membranous	0
		Wild -type	Wild-type	Membranous	0
14 months	Murine serrated lesion	c.110C > T	p.Ser37Phe	Nuclear	3
		c.110C > T	p.Ser37Phe	Nuclear	6
		c.95A > G	p.Asp32Gly	Nuclear	3
		c.69_104delCCACTGGCAGCAGCAGTCTTACTTGGATTCTGGAAT	p.Ser23_Ile35del	Nuclear	9
		c.98C > A	p.Ser33Tyr	Nuclear	3
		c.122C > T	p.Thr41Ile	Nuclear	3
		c.110C > T	p.Ser37Phe	Nuclear	3
14 months	Carcinoma	c.98C > T	p.Ser33Phe	Nuclear	9
		c.110C > T	p.Ser37Phe	Nuclear	6
		Wild-type	Wild-type	Nuclear	6
		c.101_103delGAA	p.Gly34_Ile35del	Nuclear	9
		c.94G > C	p.Asp32His	Nuclear	9
		c.98C > T	p.Ser33Phe	Nuclear	6

An overall nuclear score was calculated by multiplying the nuclear extent and intensity. β-catenin staining was considered nuclear if the score was ≥ 2. A qualitative measure for the score was based on 0 = no staining; 1–4 = low; 5–8 = moderate; and 9–12 = high.

and carcinoma (Figure 3). There was no marked difference between samples from mice that had been exposed to mutant *Braf* for 10 or 14 months prior to sacrifice. Differential gene expression was assessed between histological phenotypes that occur during tumorigenesis (wild type vs hyperplasia; hyperplasia vs mSL; mSL vs carcinoma). Between wild type mucosa and hyperplasia there were 1322 genes that were differentially expressed. The majority (n = 1112) were downregulated with the activation of mutant *Braf,* in comparison to 210 genes that had increased expression. The greatest difference (n = 3077) in expression alterations occurred with the progression of hyperplasia to mSL, in which 1880 genes were upregulated and 1197 genes were downregulated. Finally, with the progression to carcinoma a total of 1105 genes were differentially expressed with 747 genes upregulated and 361 downregulated between mSL and carcinoma.

Gene set enrichment analysis to identify significantly altered pathways associated with progression of serrated neoplasia

Expression data were analyzed with single sample gene set enrichment analysis (ssGSEA) to link gene expression changes to known biological processes [20]. ssGSEA identified alterations in a number of hallmarks with the top 20 most significant summarized in Figure 4. There was an increase in enrichment score for canonical pathways (WNT/β-catenin $P = 3.12 \times 10^{-7}$, TGF-β $P = 5.43 \times 10^{-7}$ and MTORC1 $P = 1.2 \times 10^{-6}$); transcription factors (MYC targets $P = 1.01 \times 10^{-6}$ and E2F targets $P = 1.03 \times 10^{-6}$); biological processes (angiogenesis $P = 1.01 \times 10^{-6}$, apoptosis $P = 1.43 \times 10^{-6}$ and epithelial mesenchymal transition $P = 4.39 \times 10^{-6}$). There was a decrease in enrichment for a number of metabolic processes such as adipogenesis ($P = 1.28 \times 10^{-6}$) and bile acid metabolism ($P = 1.25 \times 10^{-6}$).

Activation of WNT/β-catenin signaling within murine serrated lesions and carcinoma

WNT/β-catenin signaling was the most significantly altered pathway in the progression of serrated neoplasia. Unsupervised hierarchical clustering of fragments per kilobase of transcript per million mapped reads (FPKM) for genes within this hallmark showed clustering of histological phenotypes (Figure 5). Hyperplastic mucosa had a similar WNT gene signature to that observed in wild type mucosa. The majority of WNT signaling related genes appeared to be predominately upregulated at the mSL stage and were conserved with the transition to carcinoma. WNT pathway genes that were significantly increased in mSL compared to hyperplasia included *Nkd1* (FC = 4.90, $P = 9.10 \times 10^{-27}$), *Lef1* (FC = 4.39, $P = 3.46 \times 10^{-22}$), *Tcf7* (FC = 3.61, $P = 3.47 \times 10^{-63}$), *Jag2* (FC = 3.14, $P = 2.60 \times 10^{-33}$), *Ccnd2* (FC = 3.12, $P = 6.15 \times 10^{-51}$), *Myc* (FC = 3.11, $P = 2.04 \times 10^{-65}$) and *Axin2* (FC = 3.10, $P = 4.17 \times 10^{-48}$), while *Dll1* (FC = 2.10, $P = 1.40 \times 10^{-17}$) was downregulated. Four of the six samples of carcinoma clustered separately from mSL and an upregulation of *Wnt6* (FC = 5.25, $P = 2.58 \times 10^{-23}$) and *Wnt5b* (FC = 2.35, $P = 9.65 \times 10^{-8}$) occurred exclusively within these carcinomas. Activation of WNT signaling can occur in human *BRAF* mutant CRC due to methylation-induced gene silencing of WNT antagonists such as secreted frizzled related proteins (*SFRP1, SFRP2,* and *SFRP5*), WNT inhibitory factor 1 (*WIF1*), Dickkopf (*DKK1, DKK2, DKK3 and DKK4*), Mutated in colorectal cancer (*MCC)* and *SOX17* [25,26]. Therefore, we investigated the expression of these Wnt antagonists in our model. *Sfrp5* was the only candidate shown to be downregulated in hyperplasia (FC = 5.89, $P = 1.27 \times 10^{-10}$), mSL (FC = 5.93, $P = 2.54 \times 10^{-14}$) and carcinoma (FC = 5.70, $P = 2.55 \times 10^{-9}$) compared to normal (Figure 5).

Aberrant translocation of β-catenin to the nucleus, as shown in immunohistochemical staining, results in β-catenin-dependent transcription of target genes such as the proto-oncogene *Myc* which was significantly upregulated between hyperplasia and mSL (FC = 3.11, $P = 2.04 \times 10^{-65}$). The significantly increased enrichment for MYC targets V2 ($P = 1.01 \times 10^{-6}$) in gene set enrichment is likely due to deregulated *Myc* expression as a consequence of β-catenin mutation that leads to increased expression of Myc target genes.

Transforming growth Factor-β and epithelial mesenchymal transition

Increased TGF-β pathway signaling was present at an early stage within mSL. Transcript expression of TGF-β pathway genes *Inha* (FC = 3.88, $P = 6.53 \times 10^{-9}$), *Inhba* (FC = 3.58, $P = 1.21 \times 10^{-14}$), *Thbs1* (FC = 2.79, $P = 5.27 \times 10^{-13}$), *Bmpr1b* (FC = 2.59, $P = 8.1 \times 10^{-5}$), *Bmp4* (FC = 2.33, $P = 1.46 \times 10^{-16}$), *Tgfb3* (FC = 2.25, $P = 7.98 \times 10^{-9}$) and *Smad9* (FC = 2.15, $P = 3.33 \times 10^{-10}$) were upreg-

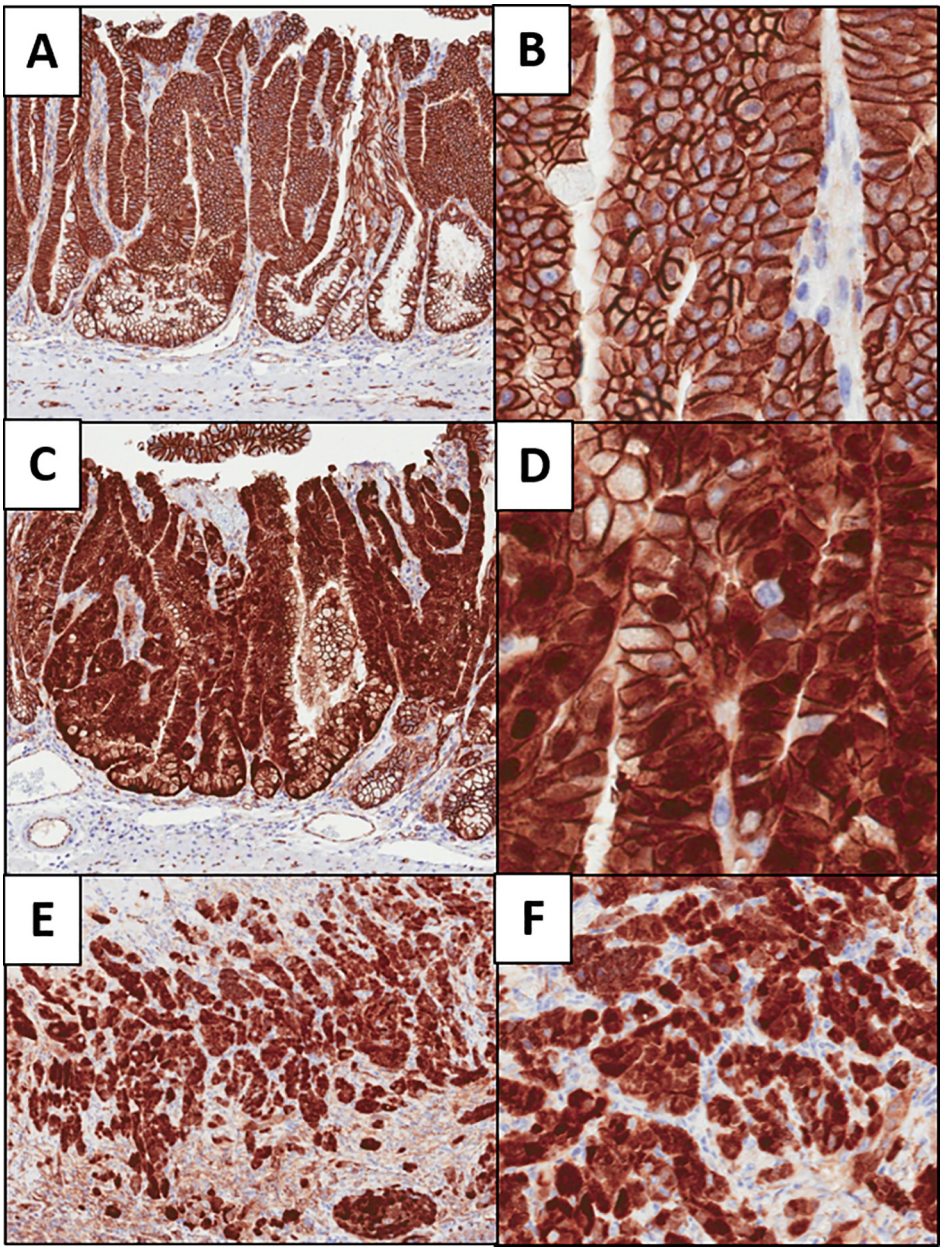

Figure 2. Murine serrated lesion showing normal membranous (A and B) and abnormal nuclear (C and D) staining of β-catenin. Carcinoma with abnormal nuclear β-catenin (E and F). A, C and E magnification ×10; B, D and F magnification ×40.

ulated in mSL compared to the background hyperplastic mucosa (Table 2). In contrast, *Bmp3* (FC = 2.38, $P = 4.73 \times 10^{-8}$) and *Acvr1c* (FC = 2.30, $P = 8.23 \times 10^{-8}$) were downregulated. With the transition to carcinoma additional TGF-β pathway genes *Serpine1* (FC = 3.41, $P = 1.23 \times 10^{-7}$), *Inhbb* (FC = 3.10, $P = 1.48 \times 10^{-6}$), *Gdf11* (FC = 2.87, $P = 2.66 \times 10^{-8}$) and *Tgfb2* (FC = 2.74, $P = 6.94 \times 10^{-7}$) were increased.

TGF-β is known to be an inducer of epithelial-mesenchymal transition, facilitating the metastatic spread of malignant cells [27]. An epithelial-mesenchymal transition signature was identified in our pathway analysis to be significantly enriched ($P = 4.39 \times 10^{-6}$) in both premalignant mSL and carcinomas (Table 2). Genes related to this biological process were discovered to be upregulated in mSL prior to transition to carcinoma. These genes included *Cd44* (FC = 4.39, $P = 1.28 \times 10^{-30}$), *Foxc2* (FC = 2.33, $P = 1.46 \times 10^{-3}$), *Snai2* (FC = 2.12, $P = 1.84 \times 10^{-12}$) and *Fn1* (FC = 2.11, $P = 1.10 \times 10^{-8}$). With the transition to carcinoma a number of additional genes were upregulated, such as *Cdh2* (FC = 3.06, $P = 1.15 \times 10^{-4}$) and *Vim* (FC = 2.27, $P = 9.57 \times 10^{-7}$).

Other key enriched pathways involved in serrated tumorigenesis

We identified a number of additional enriched pathways that may contribute to facilitating tumour growth and metastasis such as angiogenesis and MTORC1 pathway (Table 3). Angiogenesis describes the formation of new blood vessels and is a hallmark of cancer progression and metastasis [28]. We observed a significant stepwise enrichment of angiogenesis from hyperplasia to mSL and then carcinoma ($P = 1.01 \times 10^{-6}$). MTORC1 signaling was significantly enriched with serrated neoplasia progression ($P = 1.2 \times 10^{-6}$) with the greatest enrichment occurring at the transition

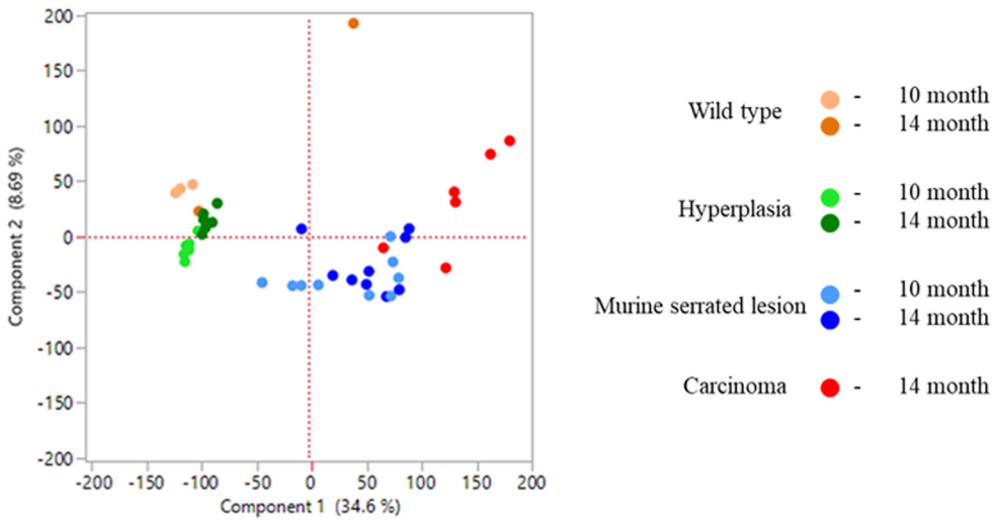

Figure 3. Principal components analysis performed on RNA sequencing data of fragments per kilobase of transcript per million mapped reads (FPKM).

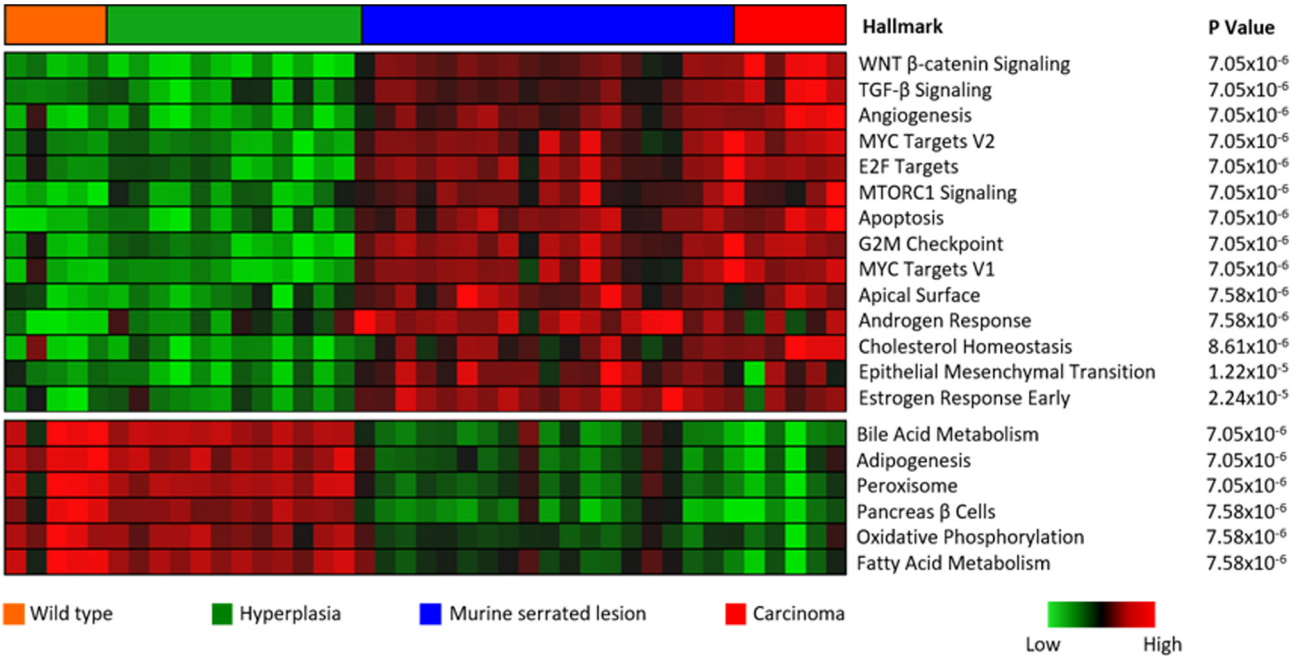

Figure 4. Heat map of top 20 most significantly altered hallmarks, ordered by in significance of enrichment for upregulated and downregulated hallmarks with progression of histological phenotypes, from single sample gene set enrichment analysis.

to mSL from hyperplasia with no further increase with the transition to carcinoma (Table 3). Targets of MTORC1 were predominately altered in mSL when compared to hyperplasia, this included overexpression of *Stc1* (FC = 3.89, $P = 5.31 \times 10^{-22}$), *Hk2* (FC = 2.46, $P = 1.23 \times 10^{-13}$) and *Mcm2* (FC = 2.20, $P = 1.76 \times 10^{-38}$). When mSL was compared with carcinoma, *Ak4* (FC = 2.88, $P = 3.42 \times 10^{-8}$), *Bcat1* (FC = 2.38, $P = 1.46 \times 10^{-3}$) and *Plod2* (FC = 2.11, $P = 7.90 \times 10^{-4}$) were additionally overexpressed.

Discussion

Our model has proven to be useful for investigating the key molecular alterations that drive the formation and progression of sessile serrated lesions to malignancy. We performed exome and RNA sequencing to investigate the molecular alterations that accompany progression of serrated lesions to malignancy. Our results showed both WNT and TGF-β signaling pathways were enriched in mSL and contributes to progression of these lesions to *Braf* mutant MSS CRC.

Aberrant activation of WNT/β-catenin is an important event in the evolution of human serrated neoplasia coinciding with the development of dysplasia [7,23]. We observed an abnormality in WNT signaling in pre-malignant mSL as a consequence of activating mutations within *Ctnnb1*, the gene encoding β-catenin. Mutation of *Ctnnb1* within exon 3 at phosphorylation or ubiquitination sites results in the stabilization of the protein and allowing translocation to the nucleus [24]. Immunohistochemical staining of β-catenin revealed an increase in nuclear β-catenin accumulation that differed notably from the typical membranous staining pattern that occurs in the absence of WNT receptor activation. Staining for

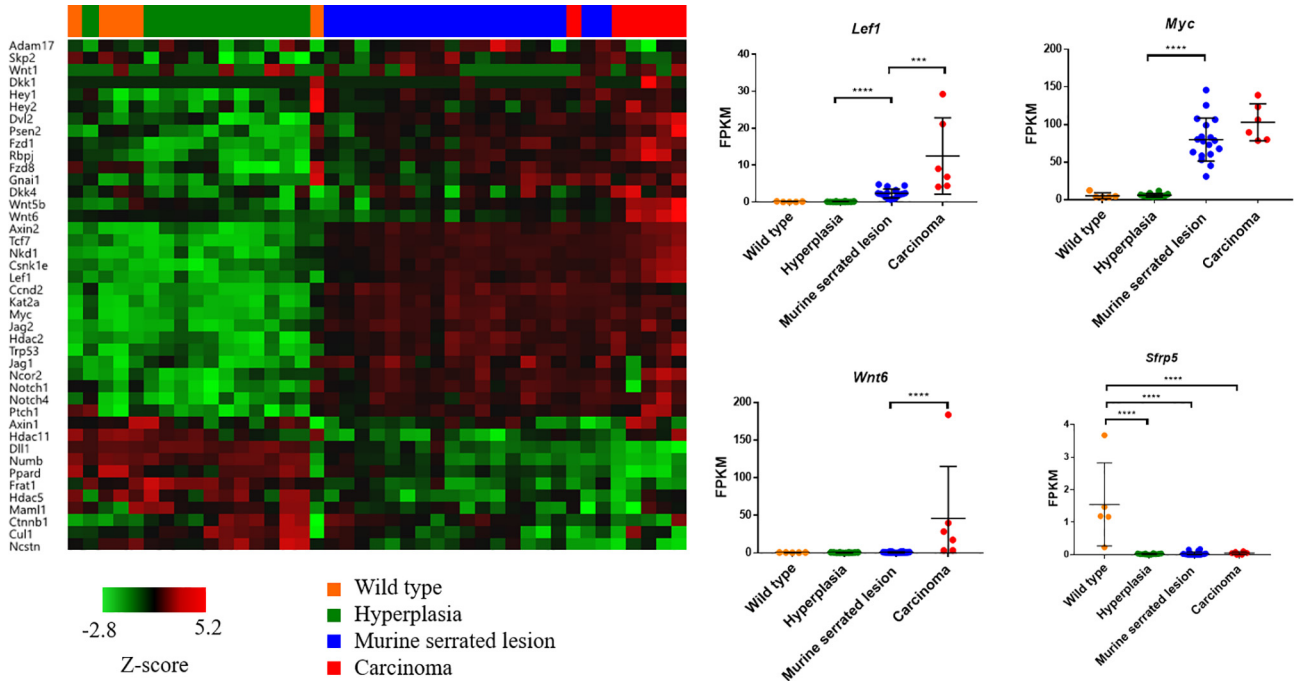

Figure 5. Unsupervised hierarchical clustering of fragments per kilobase of transcript per million mapped reads (FPKM) for genes in the WNT/β-catenin signaling pathway.

Table 2. Differentially expressed genes in each histological comparison in TGF-β and EMT pathways identified in single sample gene set enrichment. Genes in bold upregulated with progression of morphology of serrated neoplasia.

Gene Set	Comparison	Differentially Expressed Genes (Log_2 Fold Change >|2|, P-value < 0.05)
TGF-β	WT* vs HP	*Inha, Bmp10, Inhbc, Nog, Bmpr1b, Gdf1, Smad9*
	HP vs mSL‡	***Inha, Inhba, Wwtr1, Thbs1, Bmpr1b, Bmp4, Tgfb3, Pmepa1, Smad9,*** *Bmp3, Acvr1c*
	mSL‡ vs CRC½	***Serpine1, Bmp15, Gdf11, Nog, Tgfb2, Cdkn1c***
Epithelial-Mesenchymal Transition	WT* vs HP	***Plaur, Capg,*** *Cthrc1, Crlf1, Col11a1, Mgp, Lox, Cdh6, Postn, Mmp3, Serpine2, Mest, Lum, Col16a1, Cdh2, Fbln2, Abi3bp, Gpx7, Sfrp1, Eno2, Cd44, Pfn2, Thbs2, Gas1, Eln, Edil3, Sntb1, Timp1, Acta2*
	HP vs mSL‡	***Cthrc1, Mmp3, Prss2, Tnfrsf11b, Pcolce2, Crlf1, Msx1, Sfrp4, Eln, Spp1, Cd44, Lox, Bdnf, Serpine2, Pthlh, Pdlim4, Timp1, Igfbp2, Lum, Mgp, Inhba, Postn, Cxcl1, Fmod, Ctgf, Basp1, Gpc1, Col16a1, Dcn, Il6, Col1a1, Lama1, Thbs1, Tgm2, Igfbp4, Cadm1, Col5a2, Loxl1, Lrrc15, Vcan, Col1a2, Htra1, Foxc2, Plaur, Plod2, Notch2, Pmepa1, Col5a3, Fbln2, Snai2, Flna, Fn1, Fgf2, Col3a1, Sfrp1, Dpysl3, Lama2,*** *Anpep, Prrx1, Fbln1, Il15, Slc6a8, Pmp22, Nt5e, Fas, Fap, Scg2*
	mSL‡ vs CRC½	***Col11a1, Il6, Mgp, Fbln2, Thbs2, Sntb1, Timp1, Serpine1, Mfap5, Cdh2, Cthrc1, Gpc1, Eno2, Fmod, Spp1, Igfbp2, Mest, Pcolce, Serpine2, Col7a1, Vim, Lgals1, Plod2,*** *Anpep*

*WT – wild type, HP – hyperplasia, ‡mSL – murine serrated lesion, ½CRC – carcinoma.

Table 3. Differentially expressed genes in each histological comparison in other significantly altered pathways identified in single sample gene set enrichment. Genes in bold upregulated with progression of morphology of serrated neoplasia.

Gene Set	Comparison	Differentially Expressed Genes (Log_2 Fold Change >|2|, P-value < 0.05)
Angiogenesis	WT* vs HP	*Postn, Lum, Vtn, Timp1*
	HP vs mSL‡	***Msx1, Spp1, Timp1, Lum, Stc1, Postn, Jag2, Ccnd2, Col5a2, Vcan, Col3a1, S100a4, Pglyrp1, Olr1***
	mSL‡ vs CRC½	***Timp1, Spp1, S100a4, Stc1***
MTORC1	WT* vs HP	***Slc7a11, Acsl3,*** *Nupr1*
	HP vs mSL‡	***Stc1, Slc7a11, Igfbp5, Vldlr, Cd9, Slc7a5, Hk2, Nupr1, Plod2, Cxcr4, Mcm2, Rrm2,*** *Trib3, Cth, Slc9a3r1, Adipor2*
	mSL‡ vs CRC½	***Ak4, Bcat1, Stc1, Plod2***

*WT – wild type, HP – hyperplasia, ‡mSL – murine serrated lesion, ½CRC – carcinoma.

nuclear β-catenin was heterogeneous both within, as well as between lesions. Interestingly, the number of nuclei with abnormal β-catenin staining increased as mSL transitioned to carcinoma suggesting that this colony of cells has a selective advantage during malignant transformation. This heterogeneous staining pattern is a likely cause of discrepancies between mutation status and staining result, as observed in a few samples.

β-catenin is the intracellular signal transducer of the WNT signaling pathway and is responsible for mediating information and altering gene

transcription. Our gene expression profiling identified that genes regulated by active WNT signaling and β-catenin-induced transcription were increased in both mSL and carcinoma. WNT signaling is known to cause over expression of the *Myc* oncogene [29] which was increased in mSL, leading to the presence of a MYC signature. Over expression of WNT signaling and MYC induction has previously been shown to increase with higher grades of malignancy during the serrated route to CRC [30]. Aberrant WNT signaling was ubiquitous in both mSL's (the analogue of advanced serrated lesions in humans) and carcinoma. Collectively these data indicate that inhibition of WNT signaling in mSL has the potential to perturb their development.

Mutation of *CTNNB1* has been observed as somatic mutations in Lynch syndrome cancers, however are infrequent in human *BRAF*-driven tumorigenesis [31]. Instead, WNT activation occurs as a result of methylation-induced silencing of WNT antagonists, such as secreted frizzled-related proteins (*SFRP1*, *SFRP2* and *SFRP5*) and mutated in colorectal cancer (*MCC*), resulting in the loss of negative feedback regulation [25]. We found significant reduction in *Sfrp5* gene expression, which we previously showed to be significantly hypermethylated in mSL and carcinomas [9]. Other notable mechanisms reported in *BRAF* mutant CRC include inactivating mutations of *RNF43* and *ZNRF3*, however we did not find these in our exome sequencing data [32].

While aberrant WNT signaling has previously been shown to occur as a late event in the development of serrated neoplasia, the role of TGF-β in *BRAF* mutant CRC is yet to be fully understood [33]. In conventional pathway cancers *SMAD4* mutation is common, suggesting a tumour suppressive role for TGF-β signaling that is overcome with disruption of the pathway early in tumorigenesis. In contrast, increased TGF-β signaling in the context of *BRAF* mutant CRC has been suggested to play a tumorigenic role, promoting malignancy. Activation of TGF-β has been shown to induce an epithelial-mesenchymal transition signature and a mesenchymal phenotype in *BRAF* mutant organoids [33]. We have shown increased TGF-β signaling in mSL and an epithelial-mesenchymal transition signature, suggesting that lesions are pre-programmed for migration early in development of cancer. Angiogenesis is a hallmark of cancer progression with the formation of new vasculature sustaining the growth of solid tumors and facilitating metastasis [28]. We noted a significant enrichment for angiogenesis in our data. The combination of both an epithelial-mesenchymal transition, likely due to TGF-β, and angiogenic signature within these lesions, may contribute to the aggressive phenotype and late-stage presentation of *BRAF* mutant MSS CRC.

Recently, the characteristics of the tumour immune microenvironment have become increasingly important with the availability of immune checkpoint therapy. The TGF-β pathway has been associated with dampening of the tumour immune microenvironment through T-cell exclusion [34,35]. The presence of a strong TGF-β signature highlighted in our study suggests that modulating this pathway may contribute to sensitizing *BRAF* mutant MSS CRC to immune checkpoint therapy, and is an important avenue of future research.

MTORC1 is downstream of the PI3K/AKT signaling pathway and is commonly overexpressed in CRC. MTORC1 is involved in controlling protein synthesis through the phosphorylation of eukaryotic translation initiation factor 4E binding protein (4E-BP1) and the p70S6 ribosomal kinase (S6K), leading to translation of oncogenes [36]. MTORC1 gene expression signature has previously been found to define a subset of *BRAF* mutant CRC. Interestingly this subset has been described to also involve the presence of an epithelial-mesenchymal transition signature and slight enrichment for MSS cancers [37]. Inhibition of MTORC1 signaling with rapamycin has been trialled in CRC [38–40]. Although limited therapeutic benefit was demonstrated in this trial, inhibition of MTORC1 in combination with other rationally selected targeted therapies may be efficacious for this cancer subgroup.

Conclusion

Analysis of exome sequencing data in combination with gene transcript expression data has provided insight into the pathways that are altered during the development of *BRAF* mutant MSS CRC. Our data show aberrant expression of both WNT and TGF-β signaling pathways, a finding that may inform future research into therapeutic strategies, leading to improved prognosis in this aggressive subgroup of CRC.

Grant support

Pathology Queensland, Cancer Council Queensland, National Health and Medical Research Council of Australia, Gastroenterological Society of Australia, RBWH Foundation, QIMR Berghofer, Australian Postgraduate Award Research Training Program Scholarship, Royal College of Pathologists of Australasia Postgraduate Research Fellowship, Tour De Cure and Australian Rotary Health.

Data availability statement

The data that support the findings of this study are available from the corresponding author upon reasonable request.

Appendix A. Supplementary data

Supplementary data to this article can be found online at https://doi.org/10.1016/j.neo.2019.12.002.

References

1. Fearon ER, Vogelstein B. A genetic model for colorectal tumorigenesis. *Cell* 1990;**61**(5):759–67.
2. Snover DC. Update on the serrated pathway to colorectal carcinoma. *Hum Pathol* 2011;**42**(1):1–10.
3. Leggett B, Whitehall V. Role of the serrated pathway in colorectal cancer pathogenesis. *Gastroenterology* 2010;**138**(6):2088–100.
4. Spring KJ, Zhao ZZ, Karamatic R, et al. High prevalence of sessile serrated adenomas with BRAF mutations: A prospective study of patients undergoing colonoscopy. *Gastroenterology* 2006;**131**(5):1400–7.
5. Weisenberger DJ, Siegmund KD, Campan M, et al. CpG island methylator phenotype underlies sporadic microsatellite instability and is tightly associated with BRAF mutation in colorectal cancer. *Nat Genet* 2006;**38**(7):787.
6. Lochhead P, Kuchiba A, Imamura Y, et al. Microsatellite instability and BRAF mutation testing in colorectal cancer prognostication. *J Natl Cancer Inst* 2013;**105**(15):1151–6.
7. Bettington M, Walker N, Rosty C, et al. Clinicopathological and molecular features of sessile serrated adenomas with dysplasia or carcinoma. *Gut* 2017;**66**(1):97.
8. Samowitz WS, Sweeney C, Herrick J, et al. Poor survival associated with the BRAF V600E mutation in microsatellite-stable colon cancers. *Cancer Res* 2005;**65**(14):6063.
9. Bond CE, Liu C, Kawamata F, et al. Oncogenic BRAF mutation induces DNA methylation changes in a murine model for human serrated colorectal neoplasia. *Epigenetics* 2018/01/02 2018,;**13**(1):40–8.
10. Rad R, Cadi·anos J, Rad L, et al. A genetic progression model of BrafV600E-induced intestinal tumorigenesis reveals targets for Therapeutic intervention. *Cancer Cell* 2013;**24**(1):15–29.
11. Martin M. Cutadapt removes adapter sequences from high-throughput sequencing reads. *EMBnet. J* 2011;**17**(1).
12. Li H. Aligning sequence reads, clone sequences and assembly contigs with BWA-MEM. *arXiv* 2013.
13. Li H, Wysoker A, Fennell T, et al. The sequence alignment/map format and SAMtools. *Bioinformatics* 2009;**25**(16).
14. Kassahn KS, Holmes O, Nones K, et al. Somatic point mutation calling in low cellularity tumors. *PLoS One* 2013;**8**(11) e74380.

15. McKenna A, Hanna M, Banks E, et al. The genome analysis toolkit: A MapReduce framework for analyzing next-generation DNA sequencing data. *Genome Res* 2010;**20**(9):1297–303.
16. Cingolani P, Platts A, Wang LL, et al. A program for annotating and predicting the effects of single nucleotide polymorphisms, SnpEff: SNPs in the genome of Drosophila melanogaster strain w1118; iso-2; iso-3. *Fly* 2012;**6**(2):80–92.
17. Dobin A, Davis CA, Schlesinger F, et al. STAR: Ultrafast universal RNA-seq aligner. *Bioinformatics* 2012;**29**(1):15–21.
18. DeLuca DS, Levin JZ, Sivachenko A, et al. RNA-SeQC: RNA-seq metrics for quality control and process optimization. *Bioinformatics (Oxford, England)* 2012;**28**(11):1530–2.
19. Li B, Dewey CN. RSEM: accurate transcript quantification from RNA-Seq data with or without a reference genome. *BMC Bioinf* 2011;**12**:323.
20. Aravind S, Pablo T, Vamsi KM, et al. Gene set enrichment analysis: A knowledge-based approach for interpreting genome-wide expression profiles. *Proc Natl Acad Sci USA* 2005;**102**(43):15545.
21. Love MI, Huber W, Anders S. Moderated estimation of fold change and dispersion for RNA-seq data with DESeq2. *Genome Biol* 2014;**15**(12) :550.
22. Mark LB, Neal IW, Christophe R, et al. A clinicopathological and molecular analysis of 200 traditional serrated adenomas. *Mod Pathol* 2014;**28**(3).
23. Borowsky J, Dumenil T, Bettington M, et al. The role of APC in WNT pathway activation in serrated neoplasia. *Mod Pathol* 2017.
24. Morin PJ, Sparks AB, Korinek V, et al. Activation of β-Catenin-Tcf signaling in colon cancer by mutations in β-Catenin or APC. *Science* 1997;**275** (5307):1787–90.
25. Murakami T, Mitomi H, Saito T, et al. Distinct WNT/β-catenin signaling activation in the serrated neoplasia pathway and the adenoma-carcinoma sequence of the colorectum. *Mod Pathol* 2015;**28**(1):146–58.
26. Suzuki H, Watkins DN, Jair K-W, et al. Epigenetic inactivation of SFRP genes allows constitutive WNT signaling in colorectal cancer. *Nat Genet* 2004;**36** (4):417–22.
27. Moustakas A, Heldin C-H. Signaling networks guiding epithelial–mesenchymal transitions during embryogenesis and cancer progression. *Cancer Sci* 2007;**98**(10):1512–20.
28. Hanahan D. Weinberg Robert a. Hallmarks of Cancer: The Next Generation. *Cell* 2011;**144**(5):646–74.
29. He T-C, Sparks A, Rago C, Hermeking H. Identification of c-MYC as a target of the APC pathway. *Science (Washington)* 1998;**281**(5382):1509–12.
30. Kriegl L, Vieth M, Kirchner T, Menssen A. Up-regulation of c-MYC and SIRT1 expression correlates with malignant transformation in the serrated route to colorectal cancer. *Oncotarget* 2012;**3**(10):1182.
31. Yachida AS, Mudali AS, Martin AS, Montgomery AE, Iacobuzio-Donahue AC. Beta-catenin nuclear labeling is a common feature of sessile serrated adenomas and correlates with early neoplastic progression after BRAF activation. *Am J Surg Pathol* 2009;**33**(12):1823–32.
32. Bond CE, McKeone DM, Kalimutho M, et al. RNF43 and ZNRF3 are commonly altered in serrated pathway colorectal tumorigenesis. *Oncotarget* 2016;**7**(43):70589–600.
33. Fessler E, Drost J, Hooff SR, et al. TGFβ signaling directs serrated adenomas to the mesenchymal colorectal cancer subtype. *EMBO Mol Med* 2016;**8**(7):745–60
34. Tauriello DVF, Palomo-Ponce S, Stork D, et al. TGFβ drives immune evasion in genetically reconstituted colon cancer metastasis. *Nature* 2018;**554**:538.
35. Mariathasan S, Turley SJ, Nickles D, et al. TGFβ attenuates tumour response to PD-L1 blockade by contributing to exclusion of T cells. *Nature* 2018;**554**:544.
36. Guertin DA, Sabatini DM. Defining the role of mTOR in cancer. *Cancer Cell* 2007;**12**(1):9–22.
37. Barras D, Missiaglia E, Wirapati P, et al. BRAF V600E Mutant Colorectal Cancer Subtypes Based on Gene Expression. *Clin Cancer Res* 2017;**23** (1):104–15.
38. Ng K, Tabernero J, Hwang J, et al. Phase II study of everolimus in patients with metastatic colorectal adenocarcinoma previously treated with bevacizumab-, fluoropyrimidine-, oxaliplatin-, and irinotecan-based regimens. *Clin Cancer Res* 2013;**19**(14):3987–95.
39. Spindler K-LG, Sorensen MM, Pallisgaard N, et al. Phase II trial of temsirolimus alone and in combination with irinotecan for KRAS mutant metastatic colorectal cancer: Outcome and results of KRAS mutational analysis in plasma. *Acta Oncol* 2013;**52**(5):963–70.
40. Wolpin BM, Ng K, Zhu AX, et al. Multicenter phase II study of tivozanib (AV-951) and everolimus (RAD001) for patients with refractory, metastatic colorectal cancer. *Oncologist* 2013;**18**(4):377–8.